# Simulations of Spatially Evolving Turbulent Boundary Layers up to $Re_\theta = 4300$

Philipp Schlatter, Qiang Li, Geert Brethouwer,
Arne V. Johansson & Dan S. Henningson

*Linné Flow Centre, KTH Mechanics*
*Osquars Backe 18, SE-100 44 Stockholm, Sweden*

## Abstract

A well-resolved large-eddy simulation (LES) of a spatially developing turbulent boundary layer under zero pressure gradient up to comparably high Reynolds numbers ($Re_\theta = 4300$) is performed. The laminar inflow is located at $Re_{\delta*} = 450$ ($Re_\theta \approx 180$), a position where natural transition to turbulence can be expected. The simulation is validated and compared extensively to both numerical data sets, i.e. a recent spatial direct numerical simulation (DNS) up to $Re_\theta = 2500$ (Schlatter et al., 2009) and available experimental measurements, e.g. the ones obtained by Österlund (1999). The goal is to provide the research community with reliable numerical data for high Reynolds-number wall-bounded turbulence, which can in turn be employed for further model development and validation, but also to contribute to the characterisation and understanding of various aspects of wall turbulence.

The results obtained via LES show that good agreement with DNS data at lower Reynolds numbers and experimental data can be obtained for both mean and fluctuating quantities. In addition, turbulence spectra characterising large-scale organisation in the flow have been computed and compared to literature results with good agreement. In particular, the near-wall streaks scaling in inner units and the outer layer large-scale structures can clearly be identified in both spanwise and temporal spectra.

*Key words:* Turbulent boundary layers, large-eddy simulation (LES), high Reynolds number.

*Email address:* `pschlatt@mech.kth.se`
(Philipp Schlatter).

# 1 Introduction

Turbulent flow around bodies with solid walls is a very important research topic today for both technical and industrial as well as environmental applications. Whereas these flows are usually occuring in complex geometries with curved surfaces leading to pressure gradients or even bluff shapes promoting separation, the two-dimensional, spatially developing, zero-pressure-gradient turbulent boundary layer on a flat plate has emerged as an important canonical flow case for theoretical, numerical as well as experimental studies. Of large interest is for example the aspect of universality of the wall-normal profile of the streamwise velocity component in the limit of high Reynolds numbers. Going back to the seminal work conducted by Theodore von Kármán in the first half of the 20th century, the so-called "law of the wall" composed of the linear region close to the wall, followed by a buffer region and logarithmic overlap region up to about 10-15% of the boundary-layer thickness, has been the centre of intense discussions, see e.g. the corresponding section in the book by Pope (2000). In recent years, several careful experiments have been conducted for this canonical flow. For instance, Österlund et al. (2000) performed extensive measurements of mean and fluctuating quantities in the MTL wind tunnel at KTH Stockholm using hot-wire and hot-film anemometry for Reynolds numbers $Re_\theta$ based on the momentum thickness $\theta$ and the freestream velocity $U_\infty$ ranging from 2530 to 27300; this data set includes five measurement positions below $Re_\theta = 6000$, which are becoming accessible to numerical simulations nowadays. Partly based on these experimental data, Monkewitz et al. (2007) have recently presented various asymptotic results for high Reynolds numbers, including the mean velocity profile.

Careful analysis (Örlü, 2009) of a large amount of literature data for (experimentally) low Reynolds number turbulent boundary-layer measurements yields that some of these data do not necessarily adhere to accurate zero-pressure-gradient equilibrium conditions and independent determination of the skin friction. Therefore, new experimental measurements in the MTL windtunnel at KTH Stockholm were performed by Örlü (2009) for a generic, two-dimensional turbulent boundary layer with special focus on equilibrium conditions, for $Re_\theta = 2331$ to 8792. Sample results have been included in Schlatter et al. (2009). This data will certainly be helpful in the future for detailed comparisons with simulation data obtained at high $Re$.

To get additional insight into the mean-flow properties of turbulent wall-bounded flows, there is increased interest in understanding the dynamics of such flows, both at large and small scales. This is highlighted by the recent article by Marusic (2009). Furthermore, initial studies by Kim and Adrian (1999) who identified very large-scale structures in pipe flows, motivated the subsequent analysis of large-scale motions in channel, pipe and boundary-layer

$Re_\theta = 300$  $Re_\theta = 1433$  $Re_\theta = 2560$  $Re_\theta = 3660$  $Re_\theta = 4307$
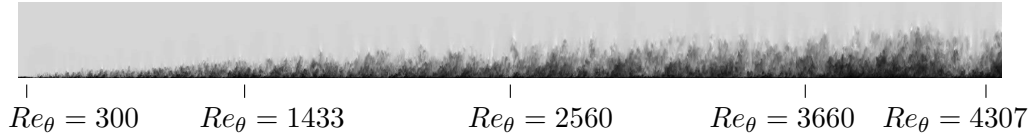
Fig. 1. Instantaneous side view with grey-scale contours of the streamwise velocity component. The domain shown corresponds to the computational box for the present LES, reaching up to approximately $Re_\theta = 4350$. Note that only half of the domain extent in the wall-normal direction is shown, and the fringe region connecting outflow and inflow is not included. The representation of the box is enlarged by a factor of four in the wall-normal direction.

flows by many authors (see e.g. Hutchins and Marusic (2007a); Guala et al. (2006); del Álamo and Jiménez (2003)).

However, as opposed to turbulent channel and pipe flow, relatively few numerical results of direct or large-eddy simulations (DNS/LES) pertaining to canonical turbulent boundary layers have been published for medium or high Reynolds numbers. In recent years, the advancement of computer technology has made it possible to perform simulations based on $\mathcal{O}(10^9)$ grid points; in channel geometry this allowed for reaching Reynolds number higher than $Re_\tau = 2000$ (based on friction velocity $U_\tau$ and channel half width $h$) by means of DNS (Hoyas and Jiménez, 2006). The spatially developing boundary-layer geometry, however, proves more difficult for accurate simulations. In particular, the long streamwise extent of the domain necessary for capturing the downstream growth of the boundary layer, and the resulting longer averaging times due to the loss of one homogeneous direction require a large computational effort even for moderate $Re$. In addition, the specification of suitable inflow and outflow conditions, and equally important, proper freestream boundary conditions are essential for a successful simulation setup.

DNS relies on resolving all relevant temporal and spatial scales on the underlying numerical grid. In LES, however, the resolution requirements can be relaxed to some extent (Sagaut, 2005). The large, energy-carrying scales of the flow are discretised on the grid and accurately simulated in both space and time, whereas the influence of the smaller scales, which are presumably more homogeneous, is modelled. For this purpose, a so-called subgrid-scale (SGS) model is then added to the equations of motion to compensate for the truncated resolution. Depending on flow case, accuracy requirements and employed SGS model, typically a reduction of the number of grid points by a factor of $\mathcal{O}(10)$ can be obtained for wall-resolved simulations compared to a DNS of the same case.

For boundary-layer flows, the DNS by Spalart (1988) using an innovative spatio-temporal approach provided valuable data at $Re_\theta = 300, 670, 1410$; this data set has been extensively used as reference for model development, and validation of experimental techniques for the last decades. As a next step,

a simulation taking into account the true growth of the boundary layer in the downstream direction has been performed by Komminaho and Skote (2002) up to $Re_\theta = 700$. This technique to include proper inflow and outflow conditions in a spatially developing setting is usually termed "spatial simulation" as opposed to flow cases with parallel mean flows such as channel or pipe flows. Very recently, Wu and Moin (2009) performed a spatial DNS of a boundary layer undergoing transition due to a periodically passing box of turbulence; the turbulent state just after transition was located $Re_\theta = 900$ close to the outlet. A similar $Re_\theta$ was also simulated spatially by Li et al. (2009); this simulation also includes the advection of passive scalars with various Prandtl numbers. Focusing on DNS of higher Reynolds numbers, Khujadze and Oberlack (2004) were using a spectral method with laminar inflow similar to the present simulation setup, however in a much shorter domain. Nevertheless, $Re_\theta = 2240$ was reached in these simulations. An even higher Reynolds number of $Re_\theta = 2900$ was reached by Ferrante and Elghobashi (2005). Their spatial simulation was not started from laminar flow, but rather from turbulent inflow conditions located at $Re_\theta = 2340$. A long domain stretching from about $Re_\theta = 1000$ to 2000 was considered in the recent simulations briefly summarised in Simens et al. (2009). Also in this case, laminar-turbulent transition is not part of the setup, and the flow is started directly from turbulent inflow conditions. Nevertheless, a comparably long adjustment and settling region at the beginning of the domain was necessary until equilibrium conditions could be assured.

A DNS using a spectral method similar to the one used by Komminaho and Skote (2002), but in a much larger computational box was recently presented by Schlatter et al. (2009), reaching $Re_\theta = 2500$ in a fully spatial setup with the (laminar) inlet located at $Re_\theta \approx 200$. A comparison with new experiments performed at the same Reynolds number revealed excellent agreement between DNS and measurements. This dataset will be used in the present work extensively to validate the chosen simulation approach.

For turbulent boundary layers, the Reynolds number $Re_\theta \approx 4300$ has to be considered at present high from a simulation point of view. Due to the difficulty of performing simulations and experiments at Reynolds numbers $Re_\theta$ on the order of a few thousand, there is a comparably large spread of the existing data in the literature for integral, mean and fluctuating turbulent quantities, see e.g. Honkan and Andreopoulos (1997). There is thus a need for accurate and reliable simulation data of spatially developing turbulent boundary layers with $Re_\theta$ to be compared to high-quality experimental results. To this end, the inflow in the numerical simulation should be positioned far enough upstream, i.e. comparable to where natural transition occurs, to ensure that the flow reaches a fully developed, undisturbed equilibrium state further downstream. However, as pointed out by Österlund et al. (2000), a clear overlap region can only be detected above $Re_\theta \approx 6000$, which might be just about to become accessible for adequately resolved transient numerical simulations.

The aim of the present study is to perform and validate well-resolved spatial large-eddy simulations (LES) in an effort to obtain accurate and reliable data at higher Reynolds numbers exceeding $Re_\theta = 2000$. A snapshot of such a simulation is presented in Fig. 1, with several relevant downstream positions indicated. The inflow is positioned at a low streamwise Reynolds number, $Re_{\delta^*} = 450$ based on the displacement thickness $\delta^*$ at the inlet. An exhaustive amount of statistics, e.g. one and two-point statistics, Reynolds-stress budgets and time series pertaining to turbulent quantities, are collected and evaluated. In the present contribution, a selection of these statistics is presented, and discussed in relation to previous numerical and experimental data.

The paper is organised as follows. In Section 2 the numerical method and the simulation parameters are introduced. Then, Section 3 discusses statistical quantities such as mean profiles, fluctuations and budgets. Spectral information about turbulent structures are introduced in Section 4. Finally, conclusions are given in Section 5.

## 2    Numerical Methodology

The simulations are performed using a fully spectral method to solve the three-dimensional, time-dependent, incompressible Navier-Stokes equations (Chevalier et al., 2007). In the wall-parallel directions, Fourier series with dealiasing are used, whereas the wall-normal direction is discretised with Chebyshev polynomials. The discretisation is based on a velocity-vorticity formulation to exactly enfore continuity. Time is advanced with a standard mixed Crank-Nicolson/Runge-Kutta scheme. The periodic boundary conditions in the streamwise direction are combined with a spatially developing boundary layer by adding a "fringe region" at the end of the domain (Bertolotti et al., 1992; Chevalier et al., 2007). In this region, the outflowing fluid is forced via a volume force to the laminar inflowing Blasius boundary-layer profile, located at $Re_{\delta_0^*} = 450$ based on the displacement thickness $\delta_0^*$ at the inlet. A low-amplitude trip force acting in the wall-normal direction is used to cause rapid laminar-turbulent transition close to the inlet (see Fig. 1). Compared to the reference DNS (Schlatter et al., 2009) the forcing amplitude is marginally reduced which leads to slightly later transition. The boundary conditions in the freestream are of Neumann type, i.e. the wall-normal variation of the velocity components is forced to zero at the upper boundary. This requirement together with incompressibility leads to a constant streamwise velocity at the upper boundary, whereas the normal velocity component might be non-zero to account for the boundary-layer growth. The spectral method provides excellent accuracy and dispersion properties as compared to low-order discretisations.

The computational domain is $x_L \times y_L \times z_L = 6000\delta_0^* \times 200\delta_0^* \times 240\delta_0^*$ with

5

$4096 \times 385 \times 384$ spectral collocation points in the streamwise, wall-normal and spanwise directions, respectively. In physical space, the number of grid points in the streamwise and spanwise direction are increased by a factor $3/2$ due to the dealiasing as mentioned above. The height of the computational domain is chosen to be at least three times the largest 99%-boundary-layer thickness $\delta_{99}$; in the spanwise direction an even larger domain has been chosen to ensure the correct development of large-scale structures scaling in outer units. The grid points are non-equidistantly distributed in the wall-normal direction, with at least 10 collocation points within the region $y^+ < 10$. The maximum grid spacing in viscous units is then $\Delta x^+ \times \Delta y^+_{\max} \times \Delta z^+ = 25.3 \times 14.2 \times 10.8$. The statistics are sampled on-the-fly over $\Delta t^+ \approx 50,000$ viscous time units, or 36 in terms of $\delta_{99}/U_\tau$ at $Re_\theta = 4300$. Owing to the high computational cost of the simulations, the numerical code is fully parallelised running on $\mathcal{O}(1000)$ processors (Li et al., 2008). In total, the present simulation required $2 \cdot 10^6$ core hours on a modern PC cluster with high-speed interconnect.

Since the chosen resolution is not fully adequate for a direct numerical simulation, the unresolved quantities have to be treated via a subgrid-scale model. In the present case, the ADM-RT model (Schlatter et al., 2004) has been employed, supplementing the governing equations with a dissipative term. The equations of motion for the resolved velocity $\overline{u}_i$ and pressure $\overline{p}$ thus read

$$\frac{\partial \overline{u}_i}{\partial t} + \overline{u}_j \frac{\partial \overline{u}_i}{\partial x_j} = -\frac{\partial \overline{p}}{\partial x_i} + \frac{1}{Re} \frac{\partial^2 \overline{u}_i}{\partial x_j \partial x_j} - \chi H_N * \overline{u}_i \ , \tag{1}$$

together with the incompressibility contraint $\partial \overline{u}_i / \partial x_i = 0$. The relaxation term $\chi H_N * \overline{u}_i$ is based on a high-order three-dimensional filter operation $H_N := (I - G)^{N+1}$ convoluted with $\overline{u}_i$. $G$ is a lower-order, low-pass filter defined in Stolz et al. (2001). The model coefficient $\chi$, having units of an inverse time, was chosen to be a constant throughout the whole flow domain, i.e. $\chi = 0.2 U_\infty / \delta_0^*$; a low sensitivity of the results to the exact value of this coefficient has already been reported by Schlatter et al. (2006) and Schlatter (2005). In addition, the order of the high-pass filter is determined by the coefficient $N$, which is chosen as $N = 5$ (Schlatter, 2005). This choice ensures that the relaxation is confined to the smallest resolved scales in the flow, and does not directly influence the larger scales.

The effect of the present SGS model is to cause fluctuations close to the numerical cutoff to be damped. This additional dissipation regularises the flow solution, and allows to perform accurate simulations of both transitional and turbulent flows at reduced resolution, in particular for simulation methods based on spectral discretisation, see e.g. Schlatter et al. (2006). Note that the ADM-RT model converges by construction towards a DNS with increasing resolution. In particular we would like to stress that the near-wall region is fully resolved in both time and space (i.e. wall-resolved LES), as opposed to more applied LES, e.g. based on wall-models (Piomelli and Balaras, 2002),

hybrid approaches such as detached-eddy simulation (DES, Spalart (2009)), or specific near-wall SGS models (Chung and Pullin, 2009).

For the present simulation case the grid resolution has been chosen to be very fine for an LES; traditional LES resolution for wall-bounded flows could be as much as two to three times lower in each direction. As e.g. shown in Schlatter et al. (2004) using the ADM-RT model accurate channel-flow statistics could be obtained even at such resolutions. It is however not the aim of the present work to validate the LES modelling per se, or to reduce the resolution as much as possible. Rather we focus on obtaining accurate simulation data at high Reynolds numbers for turbulent boundary layers, which can then be further analysed and used as reference data.

## 3   Averaged Results

As mentioned above, the laminar inflow for the present simulation is located at $Re_{\delta^*} = 450$, roughly corresponding to $Re_\theta = 180$, which is low enough to ensure a physical flow development further downstream, see also Fig. 1. Once a statistically stationary state has been reached, statististics are averaged over the spanwise direction $z$ and time $t$. Thus the Reynolds decomposition

$$u = \langle u \rangle + u' = U + u' \tag{2}$$

is used, the brackets $\langle \cdot \rangle$ indicating the average in $z$ and $t$. Note that throughout this paper only resolved quantities are considered; subgrid-scale contributions are not added onto e.g. the turbulent stresses. Based on the mean velocity profile $U(x, y)$ the shear stress at the wall is obtained as $\tau_w(x) = \mu(\mathrm{d}U/\mathrm{d}y)|_{y=0}$. Following the classical theory of turbulent boundary layers (see e.g. Pope, 2000), the friction velocity $U_\tau$ provides the relevant velocity scale throughout the boundary layer, whereas the viscous length scale $\ell_\star$ is the characteristic length at least close to the wall. The scaled quantities in wall scaling are thus written as, e.g., $U^+ = U/U_\tau$ and $y^+ = y/\ell_\star$.

The various Reynolds numbers in the present spatially evolving boundary-layer flow are shown in Figure 2, in particular $Re_\theta \equiv U_\infty \theta/\nu$ based on the free-stream velocity $U_\infty$ and the momentum thickness

$$\theta \equiv \int_0^\infty \frac{U}{U_\infty} \left( 1 - \frac{U}{U_\infty} \right) \mathrm{d}y \ , \tag{3}$$

the Reynolds number $Re_\delta^* \equiv U_\infty \delta^*/\nu$ based on the displacement thickness

$$\delta^* \equiv \int_0^\infty \left( 1 - \frac{U}{U_\infty} \right) \mathrm{d}y \ , \tag{4}$$
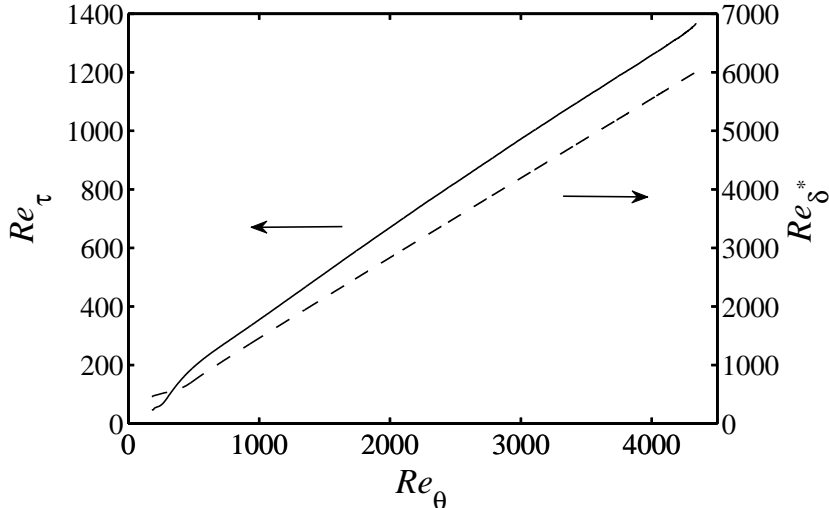
Fig. 2. Reynolds numbers for the present spatially evolving flow: —— $Re_\tau \equiv U_\tau \delta_{99}/\nu$ based on the friction velocity $U_\tau$ and 99%-boundary-layer thickness $\delta_{99}$, ---- $Re_{\delta*} \equiv U_\infty \delta^*/\nu$ based on free-stream velocity $U_\infty$ and displacement thickness $\delta^*$ as a function of $Re_\theta \equiv U_\infty \theta/\nu$ based on momentum thickness $\theta$.

and $Re_\tau \equiv U_\tau \delta_{99}/\nu$ based on the friction velocity $U_\tau$ and the 99%-boundary-layer thickness $\delta_{99}$. The computational inflow is located at $Re_{\delta*} = 450$, corresponding to a (laminar) $Re_\theta = 180$ and $Re_\tau = 45$. The usable region (see discussion below) extends to $Re_\theta = 4350$, $Re_\tau = 1370$ or $Re_{\delta*} = 6000$.

First, integral quantities of the boundary layer such as the friction coefficient are presented. Then, the mean velocity profile and profiles and budgets of turbulent fluctuating quantities are discussed. Section 4 is devoted to an analysis of the turbulent structures.

The skin-friction coefficient $c_f$ is shown in Fig. 3. The transitional region at the beginning of the domain is clearly visible. According to the computed value of $c_f$ the LES is seen to reach a fully-developed state around $Re_\theta \approx 700$. The comparison of the LES data with two data sets obtained from DNS (Schlatter et al., 2009; Li et al., 2009) is very good. Note that both DNS data were obtained based on a similar numerical setup as the present LES; however in the LES the trip forcing amplitude was slightly reduced in order to have a smoother laminar-turbulent transition close to the inlet. This is clearly visible in Fig. 3 and subsequent figures as a tendency of the LES to approach the fully developed turbulent state later than the reference DNS. Somewhat surprisingly, the comparably simple empirical correlation $c_f = 0.024 Re_\theta^{(-1/4)}$ (Kays and Crawford, 1993) provides an accurate fit to the present LES data for the range of Reynolds numbers considered; this has already been observed for the DNS data. On the other hand, the correlation $c_f = 2[(1/0.38)\log Re_\theta + 4.08]^{-2}$ based on the logarithmic region (Österlund, 1999) is marginally underpredict-
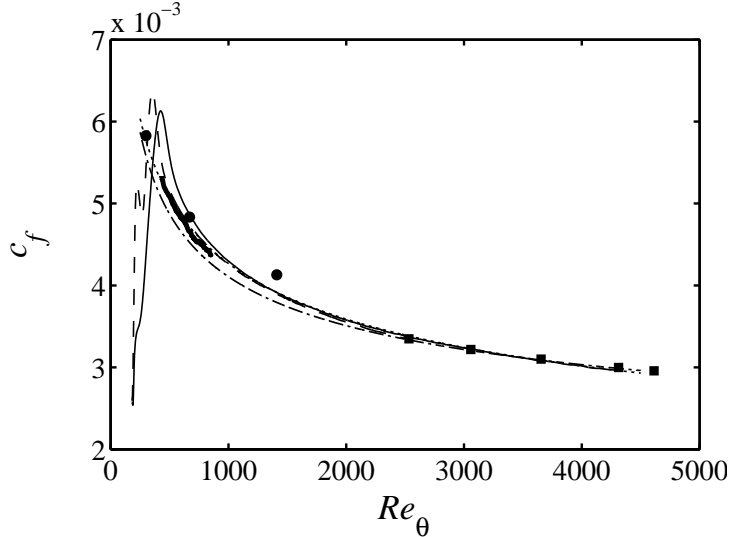
Fig. 3. Skin-friction coefficient $c_f$ as a function of $Re_\theta$. —— present LES, - - - - DNS (Schlatter et al., 2009), ········ $c_f = 0.024 Re_\theta^{(-1/4)}$ (Kays and Crawford, 1993), — · — $c_f = 2[(1/0.38)\log Re_\theta + 4.08]^{-2}$ (Österlund, 1999). • DNS by Spalart (1988), ■ experimental results by Österlund (1999), —— DNS by Li et al. (2009).

ing the friction for lower $Re$. The agreement, however, with the experimental measurement points (Österlund, 1999) in the range $Re_\theta = 2500$ to 4300 is very good. Recall that experimentally the skin friction is obtained using an oil-film technique which is independent of the hot-wire velocity measurements. For comparison, the data points of the DNS by Spalart (1988) are also shown in Fig. 3. In this case, the skin friction is overpredicted by approximately 5% at his highest $Re_\theta = 1410$. This might be a residual effect of the spatio-temporal approach employed for the simulation, which does not extend to higher Reynolds numbers.

The shape factor $H_{12} = \delta^*/\theta$, defined as the ratio of displacement $\delta^*$ to momentum thickness $\theta$, is shown in Fig. 4; $H_{12}$ is often used as an easy way of characterising the state of development of a boundary layer. Moreover, it has been shown that $H_{12}$ is a sensitive indicator of the quality of the boundary-layer data (Chauhan et al., 2008). In Fig. 4 it can again be seen that the LES is undergoing transition later than the DNS as mentioned above, and consequently approaches a fully developed state later; it is interesting to note that this state can be estimated to be reached at about $Re_\theta \approx 900$. This number appears to be slightly higher than what has been estimated for $c_f$; this further indicates that the region close to the wall is reaching a fully turbulent state earlier than the region further away from the wall. Therefore, for the present simulation the boundary layer can be assumed to be in equilibrium for an extended range of Reynolds numbers of about $Re_\theta = 900 - 4300$, which corresponds to $Re_\tau = 350 - 1350$ with $Re_\tau$ being based on the boundary-layer thickness $\delta_{99}$.

9
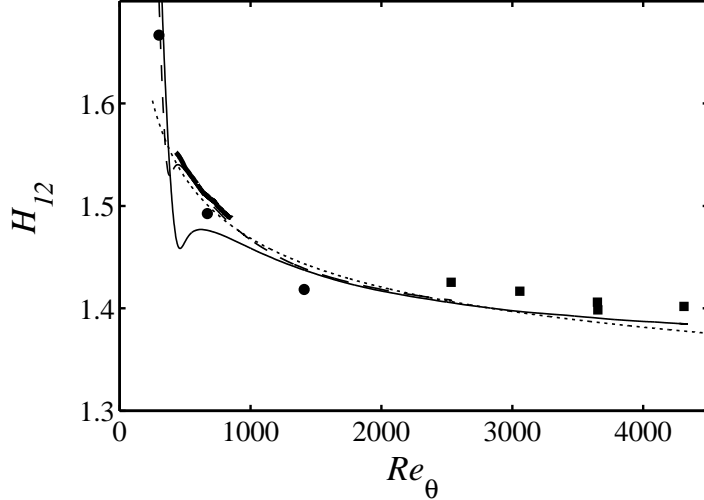
Fig. 4. Shape factor $H_{12}$ as a function of $Re_\theta$. —— present LES, - - - - DNS (Schlatter et al., 2009), ········ correlation by Monkewitz et al. (2007), ● DNS by Spalart (1988), ■ experimental results by Österlund (1999), —— DNS by Li et al. (2009).

Profiles of the mean velocity scaled in viscous units $U^+(y^+)$ obtained from the present LES are shown in Figure 5. For comparison, both DNS data from Spalart (1988) and Schlatter et al. (2009) and experimental results by Österlund (1999) are shown as well. The similarity at the higher Reynolds numbers, i.e. $Re_\theta = 2500 - 4300$, is very satisfactory. In particular, the scaled $U_\infty^+$ in the freestream is accurately predicted by the simulation, and the onset and general shape of the wake region matches the one from the experiment. However, there is a discrepancy between the present simulation data and that of Spalart highest Reynolds number, $Re_\theta = 1410$. This difference might again be attributed to the spatio-temporal simulation approach in the latter. In addition, at $Re_\theta = 2500$ there is virtually no difference between the DNS and the present LES, which indicates that the mean flow is well captured even by the lower resolution LES. In the near-wall region, all data collapse nicely on the linear relation $U^+ = y^+$ as expected according to the expansions in the viscous sublayer. In the figure, the von Kármán coefficient $\kappa$ used to indicate the logarithmic region $(1/\kappa) \log y^+ + B$ is chosen as $\kappa = 0.41$ which seems to be a good compromise for the present $Re_\theta$.

The log-law indicator function $\Xi = y^+(\mathrm{d}U^+/\mathrm{d}y^+)$ is presented in Fig. 6. The general shape of the composite profile proposed by Monkewitz et al. (2007) is followed up to $y/\delta_{99} \approx \mathcal{O}(0.1)$, the position where the wake region is expected to begin (indicated by the symbol ● in the Figure). In the overlap region $\Xi$ essentially measures the (inverse) von Kármán constant $\kappa$. From the present data, the minimum of $\Xi$ is reached at $y^+ \approx 70$ with a value of $1/\Xi \approx 0.428$ in good agreement with the prediction by Monkewitz et al. (2007), but also DNS results in both channel and boundary layers. The higher the Reynolds number, the longer the present LES data follows the composite profile, including the
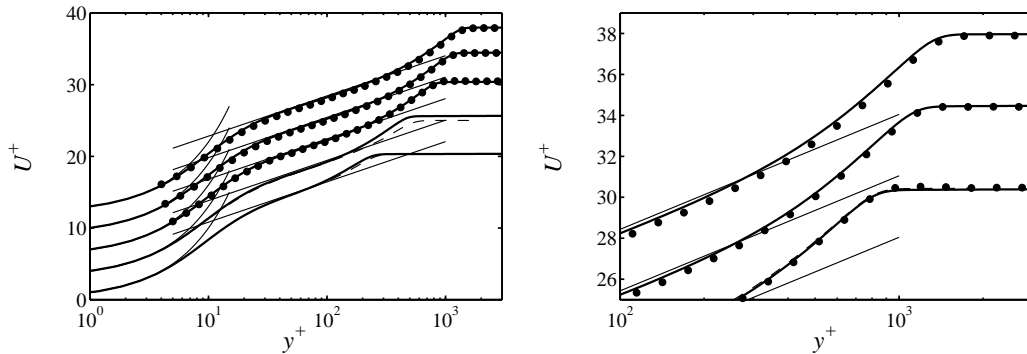
Fig. 5. Mean velocity profile $U^+$ in viscous units for ——present LES at $Re_\theta = 685, 1433, 2560, 3660, 4307$, ● measurements by Österlund (1999) at $Re_\theta = 2532, 3651, 4312$. ----DNS by Spalart (1988) at $Re_\theta = 670, 1410$, and DNS by Schlatter et al. (2009) at $Re_\theta = 2511$ (practically invisible). The profiles are shifted by $U^+ = 3$ along the ordinate for increasing $Re_\theta$. The linear and logarithmic regions are indicated by a thin line, using $1/\kappa \log y^+ + B$ with $\kappa = 0.41$ and $B = 5.2$.

decreasing $\kappa$ (increasing $\Xi$) after the minimum at $y^+ \approx 70$. However, even $Re_\theta = 4300$ is too low to reach an asymptotical logarithmic region (Österlund et al., 2000) with the proposed $\kappa \approx 0.38$. $\Xi$ in the wake region shows a clear trend towards higher maxima for increasing $Re$. In addition, it is interesting to note that in the inner region ($y^+ \approx 10$) the channel data by Hoyas and Jiménez (2006) features a slightly larger $\Xi$ than the boundary-layer data. This behaviour is similar to a boundary layer under (weak) favourable pressure gradient (Schlatter and Brandt, 2008), which demonstrates the sensitivity of the near-wall region to possible pressure gradients (Nickels, 2004).

The velocity fluctuations, e.g. $u_{\text{rms}} = \sqrt{\langle u'u' \rangle}$, and the Reynolds shear stress $\langle u'v' \rangle$ are depicted in Figure 7 in wall scaling. The agreement between the LES and DNS at $Re_\theta = 2500$ is good; slight differences can be observed for the high fluctuation regions close to the wall, in which the LES tends to underpredict the maxima by 1-2 percent. A similar issue related to the spanwise resolution is further discussed in connection with Fig. 17 further down.

As mentioned in many studies, there is only incomplete collapse in inner scaling (see e.g. Hoyas and Jiménez, 2006), most dominantly for the streamwise and spanwise fluctuations. In particular, the maximum wall-normal value of $u_{\text{rms}}$ is constantly increasing with $Re$ as shown in e.g. Metzger and Klewicki (2001); Marusic and Kunkel (2003), as well as in channel-flow simulation results. On the other hand, the total shear stress, $-\langle u'v' \rangle + (1/Re)\mathrm{d}\langle U \rangle/\mathrm{d}y$, scales very well in outer length units for the considered range of $Re_\theta$, and is therefore not shown.

The fluctuation of the wall-normal gradient of the velocity, i.e. the fluctuating streamwise wall-shear stress $\tau_w$ is considered in Fig. 8. As shown by Alfredsson

11
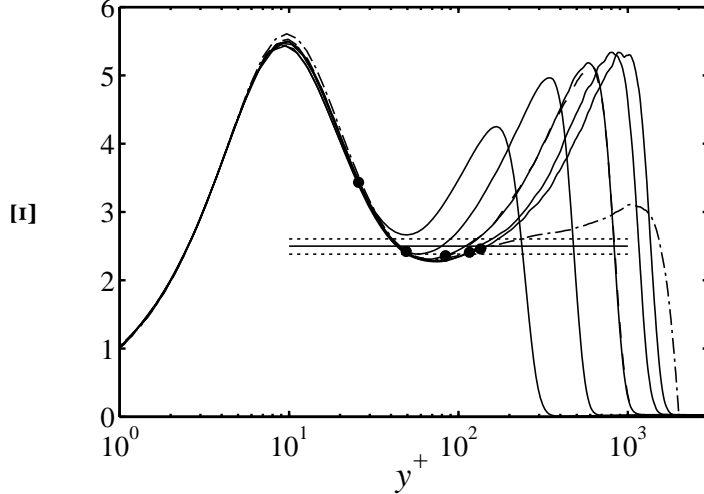
Fig. 6. Indicator function $\Xi = y^+(\mathrm{d}U^+/\mathrm{d}y^+)$ for increasing $Re_\theta = 685, 1433, 2560, 3660, 4307$. —— present LES, - - - - DNS (Schlatter et al., 2009). −·− DNS of channel flow (Hoyas and Jiménez, 2006). The horizontal lines correspond to a von Kármán contant of $1/\kappa = 1/0.38$, $1/0.4$ and $1/0.42$, respectively. The symbol ● corresponds to $0.1\delta_{99}$ for each respective $Re$.
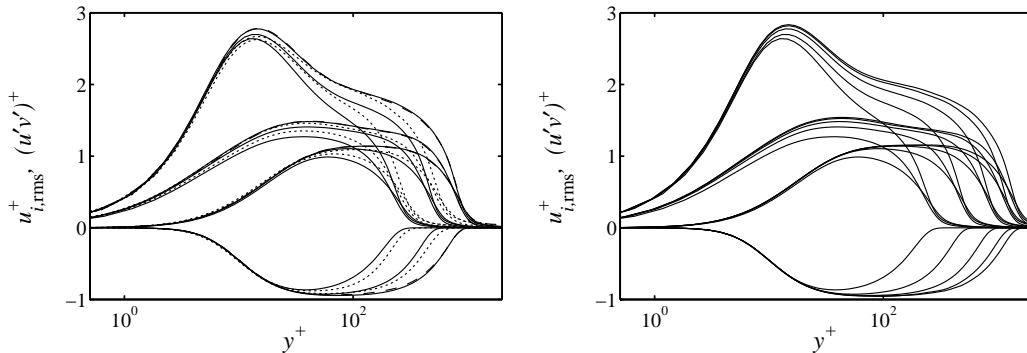


Fig. 7. *Left:* (Resolved) Reynolds stresses for the —— present LES at $Re_\theta = 685, 1433, 2560$, ········· Spalart (1988) at $Re_\theta = 670, 1410$ and - - - - Schlatter et al. (2009). *Right:* Reynolds stresses for $Re_\theta = 685, 1433, 2560, 3660, 4307$.

et al. (1988) in good agreement with data obtained by various experimental techniques and simulation approaches, $\tau_{\mathrm{rms}}^+ \approx 0.4$ in wall-bounded flow. For the present LES, a $Re$-dependence is clearly found. A new fit

$$\tau_{w,\mathrm{rms}} = 0.0155 \log Re_\tau + 0.317 \qquad (5)$$

describes the present data. Here, $Re_\tau$ is based on the friction velocity $U_\tau$ and the boundary-layer thickness $\delta_{99}$ or the channel half-width $h$. The correlation provides a reasonable description for Spalart's DNS and various channel-flow simulations (see also e.g. Abe et al., 2004). However, the data point obtained from the DNS by Wu and Moin (2009) clearly shows a higher value. This suggests that these data are in fact not fully-developed turbulence, but rather
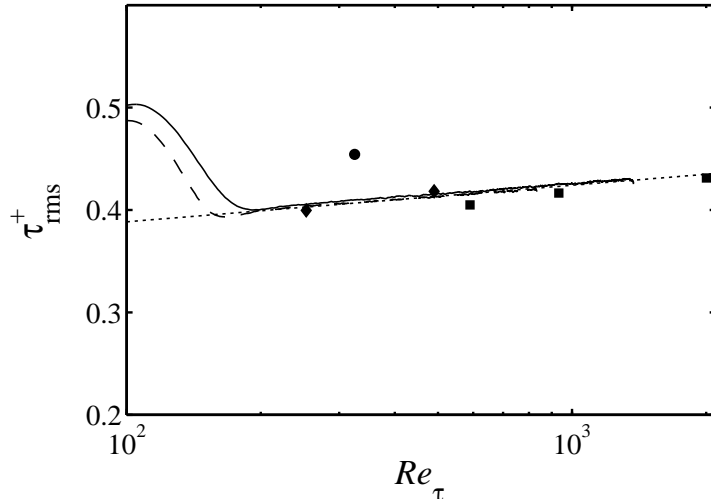
Fig. 8. Fluctuations of the wall shear stress $\tau_{\mathrm{rms}}$ for ——— present LES, - - - - DNS Schlatter et al. (2009), $\diamond$ DNS by Spalart (1988), $\bullet$ DNS by Wu and Moin (2009), $\blacksquare$ DNS of channel flow (Moser et al., 1999; del Álamo et al., 2004). ········ Fit to present data: $0.0155 \log Re_\tau + 0.317$.

transitional in nature; also for the present boundary-layer data, a higher $\tau_{\mathrm{rms}}^+$ is obtained shortly after transition.

Based on the simulation results, the individual terms in the von Kármán integral equation, here written for a zero-pressure-gradient boundary layer,

$$u_\tau^2 = U_\infty^2 \frac{\mathrm{d}\theta}{\mathrm{d}x} + \frac{\mathrm{d}}{\mathrm{d}x} \int_0^\infty \left( \langle u'^2 \rangle - \langle v'^2 \rangle \right) \mathrm{d}y \ , \tag{6}$$

relating the local skin friction to the growth of the momentum thickness $\theta$, may be considered, see Fig. 9. It turns out that the term $U_\infty^2 \mathrm{d}\theta/\mathrm{d}x$ is $\mathcal{O}(50)$ times larger than the second relevant term, the integrated normal-stress difference. On the other hand, the expressions on both sides of the equation sign balance each other to within less than 0.5%. In addition, Fig. 9 also provides a practical measure for the useful region of the simulation, i.e. the region in which an equilibrium turbulent boundary layer adhering to the boundary-layer equations is recovered. For the present case, $Re_\theta = 900 - 4100$ can be estimated, with an increasing departure for higher $Re_\theta$ (see also comments to Figs. 3 and 4 above).

Particularly in the modelling community, there is considerable interest in data pertaining to the behaviour of the pressure and its fluctuations throughout the boundary layer. Experimentally, it is very difficult to accurately measure the pressure (Tsuji et al., 2007). In Fig. 10 the wall-pressure fluctuations are shown, and Fig. 11 provides wall-normal profiles of $p_{\mathrm{rms}}$ with different scalings. Although the pressure in an incompressible LES is strictly not a well-defined quantity as it might contain subgrid-scale contributions, the agreement

13
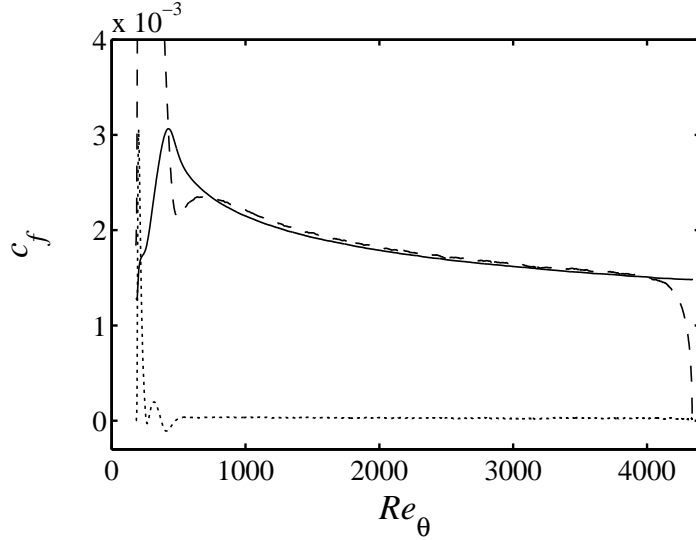
Fig. 9. —— Skin friction coefficient $c_f$ compared to the individual terms of the von Kármán equation: ········ integral of the normal-stress difference, - - - - $U_\infty^2 d\theta/dx$.
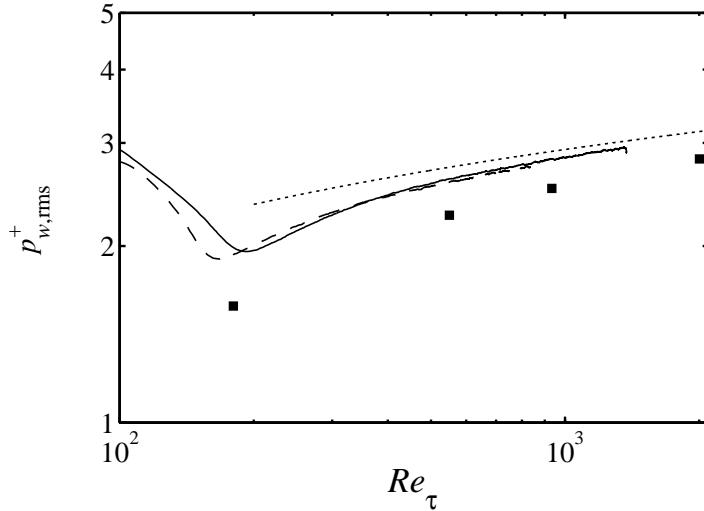


Fig. 10. —— Pressure fluctuations at the wall $p_{w,\mathrm{rms}}^+$ as a function of the friction Reynolds number $Re_\tau$, —— present LES, - - - - DNS Schlatter et al. (2009), ········ $(p_{w,\mathrm{rms}}^+)^2 = 6.5 + 1.86 \log(Re_\tau/333)$ (Farabee and Casarella, 1991). ■ DNS of channel flow (Moser et al., 1999; del Álamo et al., 2004; Hoyas and Jiménez, 2006).

between DNS and LES at $Re_\theta = 2500$ is statisfactory. It can further be seen that a mixed scaling $p_{w,\mathrm{rms}}/(U_\tau \cdot U_\infty)$ is most appropriate close to the wall, reaching a value of approximately $p_{w,\mathrm{rms}} \approx 0.11 U_\tau U_\infty$ at the wall $y = 0$. In pure inner scaling, a collapse of the data at various $Re_\theta > 1000$ can be seen for $y^+ > 200$. At the wall, $p_{\mathrm{rms}}$ is approximately 10% higher than the pressure fluctuations in channel flow at a corresponding $Re_\tau$.

In addition to the various mean and fluctuating quantities, of which a selection

14
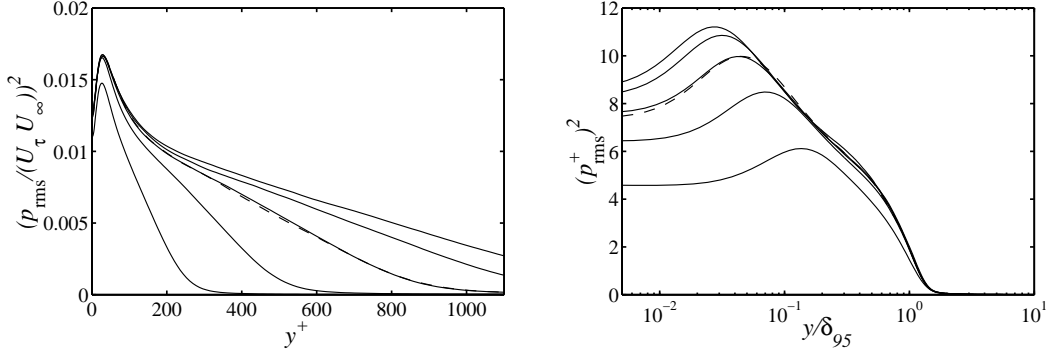
Fig. 11. —— Wall-normal profiles of the pressure fluctuations for the present LES at $Re_\theta = 685, 1433, 2560, 3660, 4307$. ----DNS Schlatter et al. (2009) at $Re_\theta = 2511$.

has already been presented, the budgets of the full Reynolds-stress tensor were computed. A sample result in Fig. 12 shows the budget of the turbulent kinetic energy $k = (1/2)\langle u_i' u_i' \rangle$. The activity of the SGS model during the simulation is clearly highlighted by the difference between the resolved dissipation and the total dissipation which includes the dissipation due to the SGS transfer. The total dissipation is computed as the residual of the energy budget when considering all relevant terms except for the SGS dissipation; when running DNS without explicit SGS model this residual is essentially zero (Li et al., 2009).

In the near-wall region this additional dissipation due to the SGS model contributes as much as 20% to the total dissipation of the turbulent energy $k$. Furthermore, the comparison of the budget terms obtained from DNS and LES compare favourably at $Re_\theta = 2100$. Close to the wall, the classical viscous scaling does show the well-known behaviour of wall-bounded flows (see e.g. Pope, 2000), and a very good collapse of the individual terms with increasing $Re$ is observed. The outer part of the boundary layer however is more interesting, as it highlights some of the major differences between internal (channel, pipe) and external wall-bounded flows. In the highly intermittent region close to the boundary-layer edge $y \sim \delta_{99}$, a new balance between turbulent diffusion as a source, and turbulent convection and velocity-pressure correlation on the loss side is established; convection is virtually absent from the near-wall region, and identically zero in parallel flows.

15
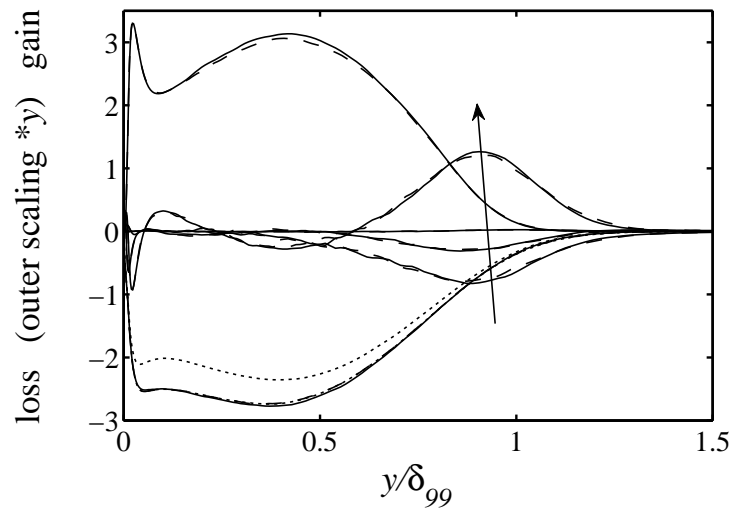
Fig. 12. Budget of the turbulent kinetic energy for ——— present LES and - - - - DNS (Schlatter et al., 2009) at $Re_\theta = 2114$. Budget terms are multiplied with $y/\delta_{99}$ and scaled in outer units $u_\tau^3/\delta_{99}$. Quantities in the direction of the arrow: Convection, dissipation (········ resolved dissipation for LES), velocity-pressure correlation, viscous diffusion, production, turbulent diffusion.

## 4 Turbulent structures

Turbulent flow is characterised by the interaction of fluctuations and eddies of various sizes, shapes and energies. It is the ensemble of these eddies that eventually lead to, e.g., the characteristic law of the wall, or the well-known profiles of the rms values. Close to the wall, the kinematic restrictions lead to the appearance of distinct flow structures which evolve with their own dynamics. The most apparent turbulent structures close to solid walls are the turbulent streaks, described and characterised by many researchers, see e.g. Kline et al. (1967); Kim et al. (1987), and more recently Lin et al. (2008). Streaks are regions of elevated or decreased velocity as compared to the local mean velocity; their size is essentially scaling in wall units, and their medium length and spacing is usually given as approximately $1000 \times 100$ wall units.

The spanwise organisation of the structures in near-wall turbulence may be considered by calculating spanwise two-point correlations $R_{\alpha\alpha}$ of a given turbulent quantity $\alpha$. In Fig. 13, the spanwise two-point correlations of the velocity components at $y^+ \approx 8$, and of the wall shear stress $\tau_w$ are shown. It can be observed that the behaviour of $R_{\tau\tau}$ and $R_{uu}$ is very similar, featuring a first minimum at $\Delta z^+ \approx 60$. The two-point correlation of the wall-normal velocity component $R_{vv}$ exhibits a strong minimum at $\Delta z^+ \approx 25$ (Kim et al., 1987), about at half the separation as for $u$. However, with increasing $Re_\theta$ the first minimum of $R_{uu}$ weakens and moves to higher values, and a second flat minimum appears at large separation $\Delta z = \mathcal{O}(\delta_{99})$ (Österlund, 1999). This indicates that superimposed onto the smaller-scale streaky structures a wider modulation must exist. Such large-scale turbulent structures have received considerable interest over the last years, both experimentally (e.g. Kim and Adrian, 1999; Guala et al., 2006; Hutchins and Marusic, 2007a) and numerically (del Álamo and Jiménez, 2003; Schlatter et al., 2009); open questions relate to the dynamic importance of these structures and possible explanations of their origin and regeneration, see e.g. the recent discussions in Hutchins and Marusic (2007b) or Mathis et al. (2009).

To further characterise the spanwise scaling, Fig. 14 shows a map of the two-point correlation of the wall-shear stress $R_{\tau\tau}$ as a function of the Reynolds number $Re_\theta$. At any sufficiently high $Re_\theta$ two minima can be discerned: The inner peak, corresponding to the near-wall streaks, can clearly be seen with a spacing of about 120 (local) wall units, as the first minimum of $R_{\tau\tau}$ at $2\Delta z^+ \approx 120$ (dashed line in Figure 14). However, a second peak (solid line) scaling as $2\Delta z \approx 0.85\delta_{99}$ is clearly visible in the two-point correlation for higher $Re_\theta$, indicating the footprint of the large-scale structures onto the fluctuating wall-shear stress. For $Re_\theta < 1000$, the two peaks merge into one and no clear separation is present. However, for $Re_\theta > 1500$ two distinct peaks can be observed. A similar plot is also shown in Schlatter et al. (2009), however being

17

restricted to $Re_\theta < 2500$. The scales measured at the wall are essentially the same in the DNS and LES.

## 4.1 Spanwise spectra

The influence of the Reynolds number on the scale separation between the small scale (inner) peak and the larger scale (outer) peak is demonstrated in Fig. 15 with the help of premultiplied spanwise spectra $k_z \Phi_{uu}(\lambda_z)/u_{\mathrm{rms}}^2$ of the streamwise velocity $u$. The small-scale peak corresponding to the streaks is
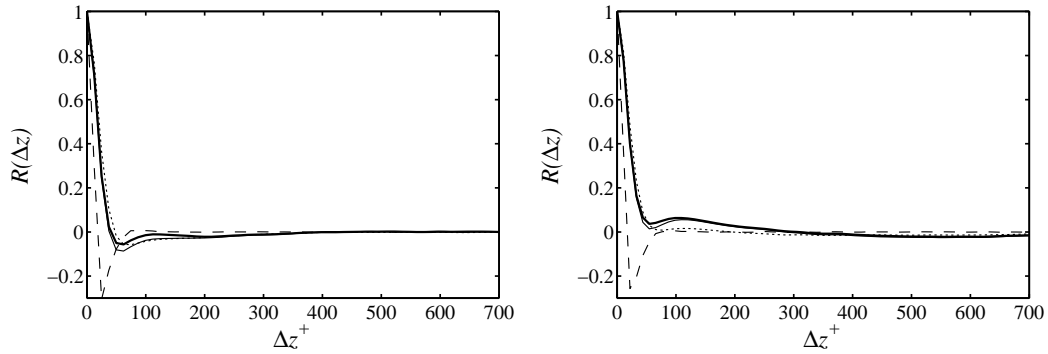


Fig. 13. Spanwise two-point correlation $R_{\alpha\alpha}(\Delta z)$ for ——— streamwise velocity $u$, - - - - wall-normal velocity $v$, $\cdots\cdots$ spanwise velocity $w$ (at $y^+ \approx 8$) and ——— the wall shear stress $\tau_w$. *Left: $Re_\theta = 1430$, Right: $Re_\theta = 4006$.*
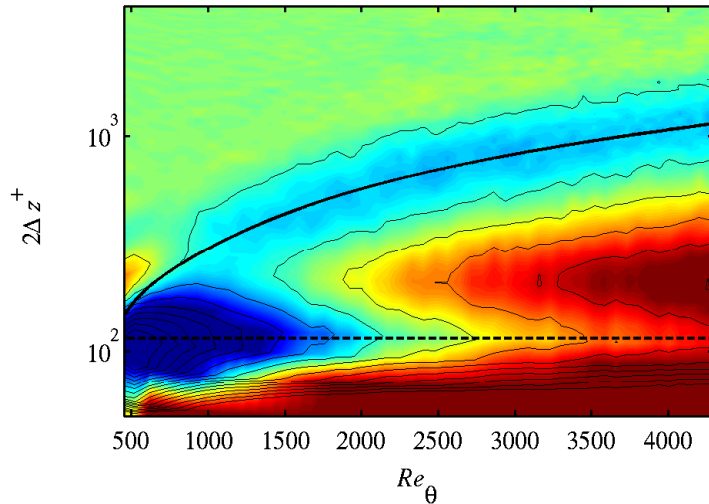


Fig. 14. Spanwise two-point correlation $R_{\tau\tau}$ of the wall-shear stress $\tau_w$ computed from the present LES. The spanwise axis is scaled by the displacement $2\Delta z$ in order to directly show the spanwise pattern spacing. ——— corresponds to $0.85\delta_{99}$, - - - - corresponds to 120 plus units. The colors range from blue ($R_{\tau\tau} \leq -0.06$) to red ($R_{\tau\tau} \geq 0.06$); contour lines go from -0.15 to 0.15 with spacing 0.02.
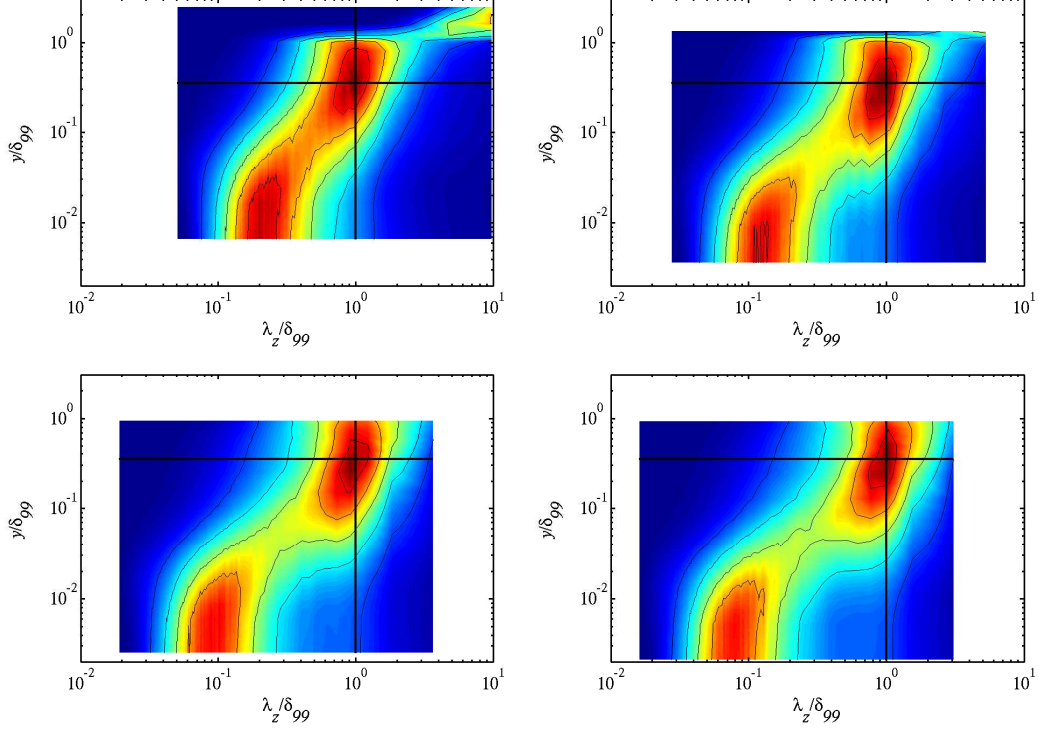
Fig. 15. Premultiplied spanwise spectra $k_z\Phi_{uu}(\lambda_z)/u_{\mathrm{rms}}^2$ of the streamwise velocity fluctuation $u$. The vertical lines indicate $\lambda_z = \delta_{99}$, the horizontal lines $y = 0.35\delta_{99}$; contour lines have a spacing of 0.1. From *left* to *right* and *top* to *bottom*: $Re_\theta = 1433, 2560, 3660, 4307$.
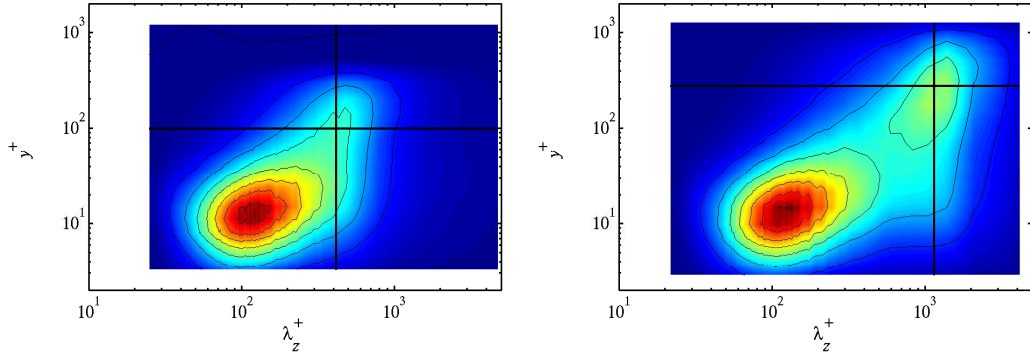


Fig. 16. Premultiplied spanwise spectra $k_z\Phi_{uu}(\lambda_z)/U_\tau^2$ of the streamwise velocity fluctuation $u$. The vertical lines indicate $\lambda_z = 0.85\delta_{99}$, the horizontal lines $y = 0.2\delta_{99}$, contour line spacing 0.5. *Top*: $Re_\theta = 1433$, *bottom*: $Re_\theta = 4307$.

centred around 120 plus units, whereas the large-scale peak is clearly scaling in outer units, i.e. attaining its maximum at a wall-normal distance of approximately $y = 0.35\delta_{99}$ with a spanwise size $\lambda_z \approx \delta_{99}$. Scaling the energy spectra with $U_\tau^2$ (Fig. 16), the inner peak features a clear maximum at $y^+ = 15$ (see e.g. del Álamo and Jiménez, 2003)), and the outer peak reaches its maximum at a wall-normal distance of approximately $0.2\delta_{99}$.
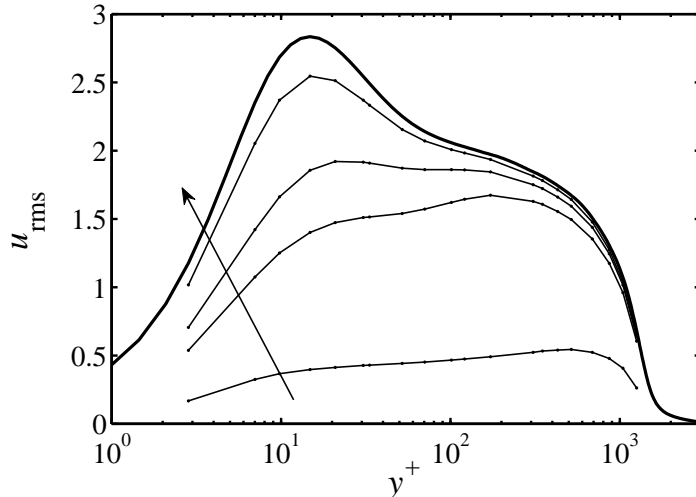
Fig. 17. Dependence of resolved $u_{\mathrm{rms}}$ fluctuations on the range of spanwise scales included at $Re_\theta = 4307$. ■■■■$u_{\mathrm{rms}}$ with full LES resolution $\Delta z^+ = 10.8$, ——— in direction of arrow: scales $\geq 2000^+$, $\geq 250^+$, $\geq 100^+$, $\geq 40^+$.

Closely connected to the spectral distribution of fluctuation energy in a signal is the way how such a signal might be measured with reduced resolution. For example, hotwire sensors have a finite length, and thus measure in fact an average signal over this specific length (Hutchins et al., 2009). This averaging operation could be simplified (i.e. by not considering any nonlinear transfer function of the wire etc.) as an integral in wavenumber space of the fluctuation energy with a lower limit that corresponds to the cutoff wavenumber (i.e. the inverse sensor length). The result of such a calculation is shown in Fig. 17 for the streamwise velocity fluctuation $u_{\mathrm{rms}}$. It becomes apparent that limiting the integration of the total fluctuations to scales larger than 40 plus units already has a significant impact on the results. In particular, for a lower limit of $\geq 250^+$, the outer peak becomes more dominant than the inner peak (Hutchins et al., 2009).

## 4.2  Temporal spectra

As opposed to channel flow computed in a (streamwise) periodic domain, the definition of streamwise spectra and thus the streamwise size of the turbulent structures is not as obvious in boundary-layer flow due to the spatial development. Usually, temporal signals are recorded at a given position, and then the Taylor hypothesis is invoked, assuming a certain convection velocity $U_c(x, y)$ in an effort to transform temporal spectra into spatial ones. This procedure naturally assumes that the convection velocity is only a function of the position, but not of the size of scales; which might not be entirely true. Therefore, in the present contribution only temporal spectra are shown, without conver-

sion into spatial spectra. Nevertheless, as a side note, the convection velocity for the present LES has been evaluated and similar results as e.g. Quadrio and Luchini (2003) have been obtained: The mean convection velocity closely follows the mean velocity profile, and levels off close to the wall with about $U_c^+ \approx 11$, featuring a small dip at $y^+ \approx 5$.

Temporal samples of the flow were recorded at various streamwise and wall-normal positions in the flow; spanning the whole spanwise extent. A first quantification of the fluctuations of such time series is given in Fig. 18 showing the probabilty density function (pdf) of the streamwise velocity at five positions from the wall to the free stream. The signal recorded closest to the wall, $y^+ = 2.8$, clearly shows a non-symmetric distribution with a large spread of velocity magnitues: Values as large as $0.5U_\infty$, but also slightly negative velocities are measured. This last observation is interesting, and preliminary visualisations show that small regions with local reversed flow are related to strong quasi-spanwise vortices in the near-wall region. As expected, the pdf's further away from the wall tend to approach a Gaussian distribution (see e.g. the pdf at $y^+ = 100$). Right at the boundary-layer edge $y = 0.9\delta_{99}$, again a non-symmetric pdf is observed, featuring a characteristic pointy tip around its maximum, $U \approx 0.992U_\infty$.

To obtain spectral information, the time series of the probe signals are subsequently transformed into Fourier space using Hanning windows based on the Welch method with up to 64 overlapping windows. In Fig. 19 premultiplied temporal spectra obtained from the present LES and the reference DNS are compared at $Re_\theta = 2500$ at various wall-normal positions. Both simulation ap-
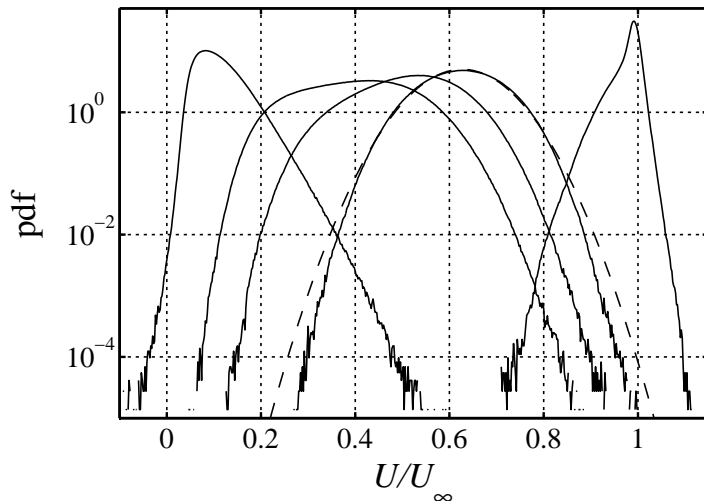


Fig. 18. Probability density functions of the streamwise velocity at $Re_\theta = 4300$ and wall-normal positions $y^+ = 2.8$, 15, 30, 100 and $y = 0.9\delta_{99}$. ----Gaussian distribution with the same parameters as the pdf at $y^+ = 100$, i.e. mean $\mu = 0.627$, variance $\sigma^2 = 0.00632$.

proaches show spectra which are very similar; the main peak at $\lambda_t \approx 3\delta_{99}/U_\infty$ (corresponding to about 1000 plus units when converted in spatial spectrum) and the flanks are accurately reproduced by the LES.

Contour plots of premultiplied temporal spectra are presented in Fig. 20 for two Reynolds numbers $Re_\theta = 1433$ and 4307. Note the good agreement of the present higher-$Re$ data to the results reported in the experimental study by Hutchins and Marusic (2007a). A fairly broad range of temporal frequencies is seen to be excited in the near-wall region ($y \approx 15$), and with higher $Re$ a tendency towards larger (i.e. longer lasting) structures is seen in the outer region $y > 0.1\delta_{99}$. The longest relevant scales can be estimated to be $\mathcal{O}(40)$ in units of $\delta_{99}/U_\infty$, however longer events $> 100\delta_{99}/U_\infty$ are also observed. The most dominant structure in the outer region is observed at a constant (temporal) period of approximately $\lambda_t = 10\delta_{99}/U_\infty$. Via the consideration of two-dimensional spectra (not shown) this structure could be identified with having a spanwise scale $\lambda_z = 0.85\delta_{99}$. Assuming a convection speed of about $0.6U_\infty$ for these large structures, a length scale $\lambda_x = 6\delta_{99}$ is obtained, which compares well to the experimental finding presented by Hutchins and Marusic (2007a) for boundary-layer flow. It should be highlighted again that for the large-scale structures an unambiguous collapse of the scales throughout the boundary layer is obtained only in the temporal spectra. The streamwise spectra (obtained by invoking Taylor's hypothesis) does not show a clear collapse of scales.
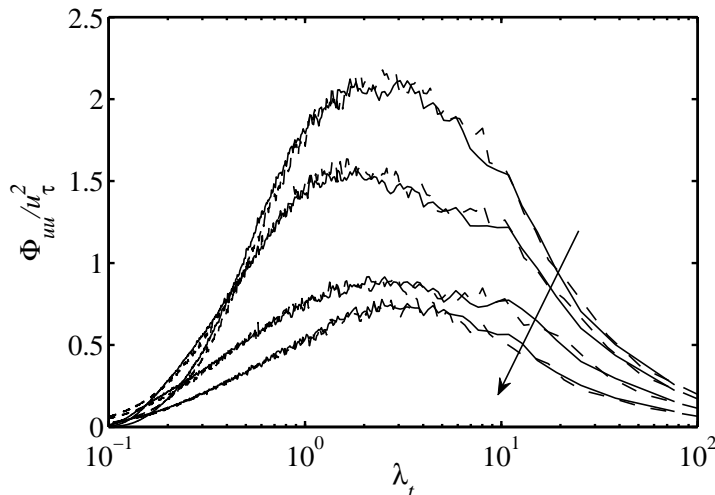


Fig. 19. One-dimensional premultiplied temporal spectrum $\omega\Phi_{uu}(\lambda_t)/U_\tau^2$ of the streamwise velocity fluctuation $u$ at $Re_\theta = 2500$ for —— present LES, - - - - DNS Schlatter et al. (2009). In direction of the arrow: $y^+ = 15, 30, 100, 300$.
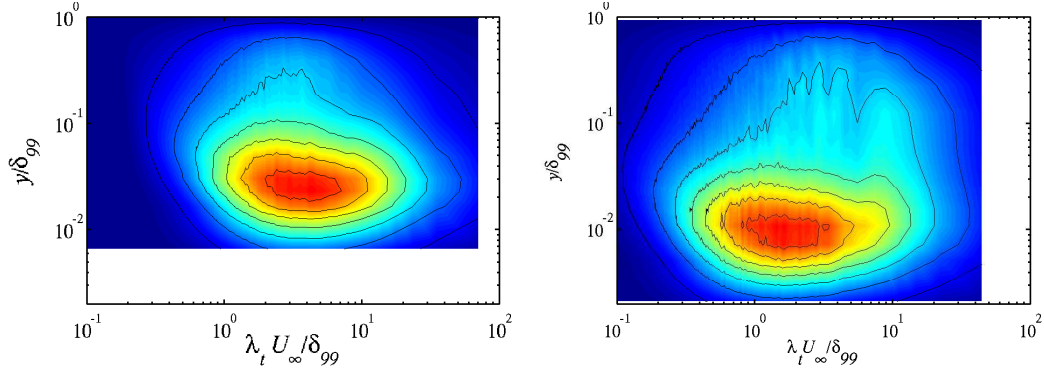
Fig. 20. Premultiplied temporal spectrum $\omega\Phi_{uu}(\lambda_t)/U_\tau^2$ of the streamwise velocity fluctuation $u$. Contour spacing 0.3. *Left*: $Re_\theta = 1433$, *right*: $Re_\theta = 4307$.

## 5   Conclusions

A well-resolved large-eddy simulation (LES) of a spatially developing turbulent boundary layer under zero pressure gradient up to (numerically) high Reynolds numbers ($Re_\theta = 4300$) is presented. The employed subgrid-scale model is the ADM-RT model (Schlatter et al., 2004), which is an efficient and simple regularisation method based on high-order filters. The (laminar) inflow is located at $Re_{\delta*} = 450$ ($Re_\theta \approx 180$), a position far enough upstream to ensure a proper flow development further downstream. Results are validated and compared extensively to both numerical data sets (Schlatter et al., 2009) and available experimental measurements, e.g. the ones obtained by Österlund et al. (2000).

The LES results are in good agreement with these existing data for both mean and fluctuating quantities, e.g. mean velocity, skin friction and fluctuating shear stress, energy budgets, pressure fluctuations, and terms in the von Kármán integral equations. In addition, spanwise and temporal correlations and spectra characterising large-scale flow organisation have been analysed. In particular, the near-wall streaks scaling in inner units and the outer layer large-scale structures can clearly be identified in both spanwise and temporal spectra. The spacing of the near-wall streaks is estimated as 120 plus units in width and about 1000 in length. The dominant large-scale structure is about $0.85\delta_{99}$ wide and persists for about $10\delta_{99}/U_\infty$ time units. A clear collapse in time scale throughout the boundary layer spanning from the wall towards the free stream could be observed.

The goal of the present study was to provide reliable numerical data for high Reynolds-number wall-bounded turbulence, which can in turn be employed for further model development and validation, but also to contribute to the further characterisation and understanding of wall turbulence, in particular boundary-layer flows. The present work summarised some of these results,

23

however the evaluation of the data base is still on-going.

The data of the present LES will be made available at `www.mech.kth.se`.

## References

Abe, H., Kawamura, H., Choi, H., 2004. Very large-scale structures and their effects on the wall shear-stress fluctuations in a turbulent channel flow up to $Re_\tau = 640$. J. Fluids Eng. 126, 835–843.

Alfredsson, P. H., Johansson, A. V., Haritonidis, J. H., Eckelmann, H., 1988. The fluctuating wall-shear stress and the velocity field in the viscous sublayer. Phys. Fluids 31 (5), 1026–1033.

Bertolotti, F. P., Herbert, T., Spalart, P. R., 1992. Linear and nonlinear stability of the Blasius boundary layer. J. Fluid Mech. 242, 441–474.

Chauhan, K. A., Monkewitz, P. A., Nagib, H. M., 2008. Criteria for assessing experiments in zero pressure gradient boundary layers. Fluid Dyn. Res. 41 (021404).

Chevalier, M., Schlatter, P., Lundbladh, A., Henningson, D. S., 2007. SIMSON - A Pseudo-Spectral Solver for Incompressible Boundary Layer Flows. Tech. Rep. TRITA-MEK 2007:07, KTH Mechanics, Stockholm, Sweden.

Chung, D., Pullin, D. I., 2009. Large-eddy simulation and wall modelling of turbulent channel flow. J. Fluid Mech. 631, 281–309.

del Álamo, J. C., Jiménez, J., 2003. Spectra of the very large anisotropic scales in turbulent channels. Phys. Fluids 15 (6), L41–L44.

del Álamo, J. C., Jiménez, J., Zandonade, P., Moser, R. D., 2004. Scaling of the energy spectra of turbulent channels. J. Fluid Mech. 500, 135–144.

Farabee, T. M., Casarella, M. J., 1991. Spectral features of wall pressure fluctuations beneath turbulent boundary layers. Phys. Fluids 3, 2410–2420.

Ferrante, A., Elghobashi, S., 2005. Reynolds number effect on drag reduction in a microbubble-laden spatially developing turbulent boundary layer. J. Fluid Mech. 543, 93–106.

Guala, M., Hommema, S. E., Adrian, R. J., 2006. Large-scale and very-large-scale motions in turbulent pipe flow. J. Fluid Mech. 554, 521–542.

Honkan, A., Andreopoulos, Y., 1997. Vorticity, strain-rate and dissipation characteristics in the near-wall region of turbulent boundary layers. J. Fluid Mech. 350, 29–96.

Hoyas, S., Jiménez, J., 2006. Scaling of the velocity fluctuations in turbulent channels up to $Re_\tau = 2003$. Phys. Fluids 18 (011702), 1–4.

Hutchins, N., Marusic, I., 2007a. Evidence of very long meandering features in the logarithmic region of turbulent boundary layers. J. Fluid Mech. 579, 1–28.

Hutchins, N., Marusic, I., 2007b. Large-scale influences in near-wall turbulence. Phil. Trans. R. Soc. A 365, 647–664.

Hutchins, N., Nickels, T. B., Marusic, I., Chong, M. S., 2009. Hot-wire spatial resolution issues in wall-bounded turbulence. J. Fluid Mech. 635, 103–136.

Kays, W. M., Crawford, M. E., 1993. Convective Heat and Mass Transfer, 3rd Edition. McGraw-Hill, New York, U.S.A.

Khujadze, G., Oberlack, M., 2004. DNS and scaling laws from new symmetry groups of ZPG turbulent boundary layer flow. Theoret. Comput. Fluid Dynamics 18, 391–411.

Kim, J., Moin, P., Moser, R., 1987. Turbulence statistics in fully developed channel flow at low Reynolds number. J. Fluid Mech. 177, 133–166.

Kim, K. C., Adrian, R. J., 1999. Very large-scale motion in the outer layer. Phys. Fluids 11 (2), 417–422.

Kline, S. J., Reynolds, W. C., Schraub, F. A., Runstadler, P. W., 1967. The structure of turbulent boundary layers. J. Fluid Mech. 30, 741–773.

Komminaho, J., Skote, M., 2002. Reynolds stress budgets in Couette and boundary layer flows. Flow Turbulence Combust. 68 (2), 167–192.

Li, Q., Schlatter, P., Brandt, L., Henningson, D. S., 2009. DNS of a spatially developing turbulent boundary layer with passive scalar transport. Int. J. Heat Fluid Flow 30, 916–929.

Li, Q., Schlatter, P., Henningson, D. S., 2008. Spectral simulations of wall-bounded flows on massively parallel computers. Tech. rep., KTH Mechanics, Stockholm, Sweden.

Lin, J., Laval, J. P., Foucaut, J. M., Stanislas, M., 2008. Quantitative characterization of coherent structures in the buffer layer of near-wall turbulence. Part 1: streaks. Exp. Fluids 45, 999–1013.

Marusic, I., 2009. Unravelling turbulence near walls. J. Fluid Mech. 630, 1–4.

Marusic, I., Kunkel, G. J., 2003. Streamwise turbulence intensity formulation for flat-plate boundary layers. Phys. Fluids 15 (8), 2461–2464.

Mathis, R., Hutchins, N., Marusic, I., 2009. Large-scale amplitude modulation of the small-scale structures in turbulent boundary layers. J. Fluid Mech. 628, 311–337.

Metzger, M. M., Klewicki, J. C., 2001. A comparative study of near-wall turbulence in high and low Reynolds number boundary layers. Phys. Fluids 13, 692.

Monkewitz, P. A., Chauhan, K. A., Nagib, H. M., 2007. Self-consistent high-Reynolds-number asymptotics for zero-pressure-gradient turbulent bound-

ary layers. Phys. Fluids 19 (115101), 1–12.

Moser, R. D., Kim, J., Mansour, N. N., 1999. Direct numerical simulation of turbulent channel flow up to $Re_\tau = 590$. Phys. Fluids 11 (4), 943–945.

Nickels, T. B., 2004. Inner scaling for wall-bounded flows subject to large pressure gradients. J. Fluid Mech. 521, 217–239.

Örlü, R., 2009. Experimental studies in jet flows and zero pressure-gradient turbulent boundary layers. Ph.D. thesis, Department of Mechanics, KTH Stockholm, Sweden.

Österlund, J. M., 1999. Experimental studies of zero pressure-gradient turbulent boundary-layer flow. Ph.D. thesis, Department of Mechanics, KTH Stockholm, Sweden.

Österlund, J. M., Johansson, A. V., Nagib, H. M., Hites, M. H., 2000. A note on the overlap region in turbulent boundary layers. Phys. Fluids 12 (1), 1–4.

Piomelli, U., Balaras, E., 2002. Wall-layer models for large-eddy simulations. Annu. Rev. Fluid Mech. 34, 349–374.

Pope, S. B., 2000. Turbulent Flows. Cambridge University Press, Cambridge, U.K.

Quadrio, M., Luchini, P., 2003. Integral space-time scales in turbulent wall flows. Phys. Fluids 15 (8), 2219–2227.

Sagaut, P., 2005. Large Eddy Simulation for Incompressible Flows, 3rd Edition. Springer, Berlin, Germany.

Schlatter, P., 2005. Large-eddy simulation of transition and turbulence in wall-bounded shear flow. Ph.D. thesis, ETH Zürich, Switzerland, Diss. ETH No. 16000, available online from `http://e-collection.ethbib.ethz.ch`.

Schlatter, P., Brandt, L., 2008. DNS of three-dimensional turbulent boundary layers. In: Armenio, V., Geurts, B. J., Fröhlich, J. (Eds.), Direct and Large-Eddy Simulation 7, September 8-10. To appear.

Schlatter, P., Örlü, R., Li, Q., Brethouwer, G., Fransson, J. H. M., Johansson, A. V., Alfredsson, P. H., Henningson, D. S., 2009. Turbulent boundary layers up to $Re_\theta = 2500$ studied through numerical simulation and experiments. Phys. Fluids 21 (051702), 1–4.

Schlatter, P., Stolz, S., Kleiser, L., 2004. LES of transitional flows using the approximate deconvolution model. Int. J. Heat Fluid Flow 25 (3), 549–558.

Schlatter, P., Stolz, S., Kleiser, L., 2006. LES of spatial transition in plane channel flow. J. Turbulence 7 (33), 1–24.

Simens, M. P., Jiménez, J., Hoyas, S., Mizuno, Y., 2009. A high-resolution code for turbulent boundary layers. J. Comput. Phys. 228, 4218–4231.

Spalart, P. R., 1988. Direct simulation of a turbulent boundary layer up to $R_\theta = 1410$. J. Fluid Mech. 187, 61–98.

Spalart, P. R., 2009. Detached-eddy simulation. Annu. Rev. Fluid Mech. 41, 181–202.

Stolz, S., Adams, N. A., Kleiser, L., 2001. An approximate deconvolution model for large-eddy simulation with application to incompressible wall-bounded flows. Phys. Fluids 13 (4), 997–1015.

Tsuji, Y., Fransson, J. H. M., Alfredsson, P. H., Johansson, A. V., 2007. Pres-

sure statistics and their scaling in high-Reynolds-number turbulent boundary layer. J. Fluid Mech. 585, 1–40.

Wu, X., Moin, P., 2009. Direct numerical simulation of turbulence in a nominally zero-pressure-gradient flat-plate boundary layer. J. Fluid Mech. 630, 5–41.